Radiation qualification and optical performance of the InGaAs type imaging sensor for the vSWIR spectral range in the VEM instrument on the VERITAS mission

A. Pohl[a], S. del Togno[b], Y. M. Rosas Ortiz[a], 'K. Westerdorff[a], C. Arcos Carrasco[a], D. Wendler[a], J. Helbert[b], G. Peter[a], I. Walter[a], P. Dern[a]
[a] Deutsches Zentrum für Luft- und Raumfahrt e.V. (DLR), Institute of Optical Sensor Systems, 12489 Berlin, Rutherfordstr. 2, Germany
[b] Deutsches Zentrum für Luft- und Raumfahrt e.V. (DLR), Institute of Planetary Research, 12489 Berlin, Rutherfordstr. 2, Germany

ABSTRACT

The Venus Emissivity Mapper (VEM) as part of NASAs Venus Emissivity, Radio science, InSAR, Topography, And Spectroscopy mission (VERITAS) is designed for mapping the surface of Venus within dedicated atmospheric spectral windows. The instrument will provide global coverage for detection of thermal emissions like volcanic activity, surface rock composition, water abundance and cloud formation as well as dynamics by observing 15 narrow filter bands in the near infrared to short wavelength infrared (NIR, SWIR) range of 862 nm to 1510 nm. An almost identical instrument will be part of ESAs EnVision mission to Venus, the VenSpec-M in the Venus Spectroscopy Suite (VenSpec). The utilized photodetector is an InGaAs type imaging sensor with integrated thermoelectric (TE) cooling. It comprises a 640x512 pixel array with 20 µm pixel pitch.

Following the mission requirements we irradiated the detector with a set of ions of various stopping powers and range distributions from lower energy Argon (Ar) to higher energy Xenon (Xe). Therefore, exploiting the mentioned ions and proper tilt angles during irradiation, our data covers a Linear Energy Transfer (LET) range of 7 to 75 MeVcm²/mg which fulfills NASA/JPL led space qualification standards (up to 75 MeVcm²/mg) as well as ESA space qualification standards (up to 60 MeVcm²/mg) for heavy-ion irradiation.

Our electrical setup consists of a dedicated over-current protection detecting high-current states occurring during irradiation steps and immediate power cycling to prevent physical damage of the device. From the event rates seen during the test we calculated the specific cross-sections and therefore can estimate the expected event rates at Venus during the mission.

The detector showed saturated cross-sections below 1E-3 cm² at 10°C with acceptable event rates for the highest LETs and our applications.

Keywords: VERITAS, VEM, EnVision, VenSpec-M, IR, SWIR, InGaAs, Imaging, Space-Qualification, Detector, FPA

1. INTRODUCTION

VERITAS and EnVision are orbital missions to Venus led by NASA and ESA respectively that will perform high-resolution radar mapping and atmospheric studies. For both missions the planetary emissivity mapper instruments will be developed by DLR, VEM for VERITAS [1] and VenSpec-M for EnVision [2] will provide near-global compositional data for the detection of thermal emissions like volcanic activity, surface rock composition, water abundance and cloud formation as well as their overall dynamics by observing 15 narrow filter bands in the near infrared to short wavelength infrared (NIR to SWIR) range of 862 nm to 1510 nm. An almost identical instrument will be part of ESAs EnVision mission to Venus the VenSpec-M in the Venus Spectroscopy Suite (VenSpec).

The photodetector utilized as a baseline for this mission is an InGaAs type imaging sensor from Xenics, model XSW-640 vSWIR, with integrated thermoelectric (TE) cooling. It comprises a 640x512 pixel array with 20 µm pixel pitch and covers a spectral range from 500 nm to 1700 nm at peak quantum efficiencies of around 80% [3].

The instrument is designed for mapping the surface of Venus within dedicated atmospheric spectral windows. It will provide global coverage for detection of thermal emissions like volcanic activity, surface rock composition, water abundance and cloud formation as well as dynamics by observing 15 narrow filter bands in the near infrared to short wavelength infrared (NIR, SWIR) range of 862 nm to 1510 nm.

Figure 1 shows a render of the instrument, specifically VenSpec-M is shown here. Light from the observed scenes on Venus enters the baffle on the left side and is transmitted through the optics to the back where the detector is located.

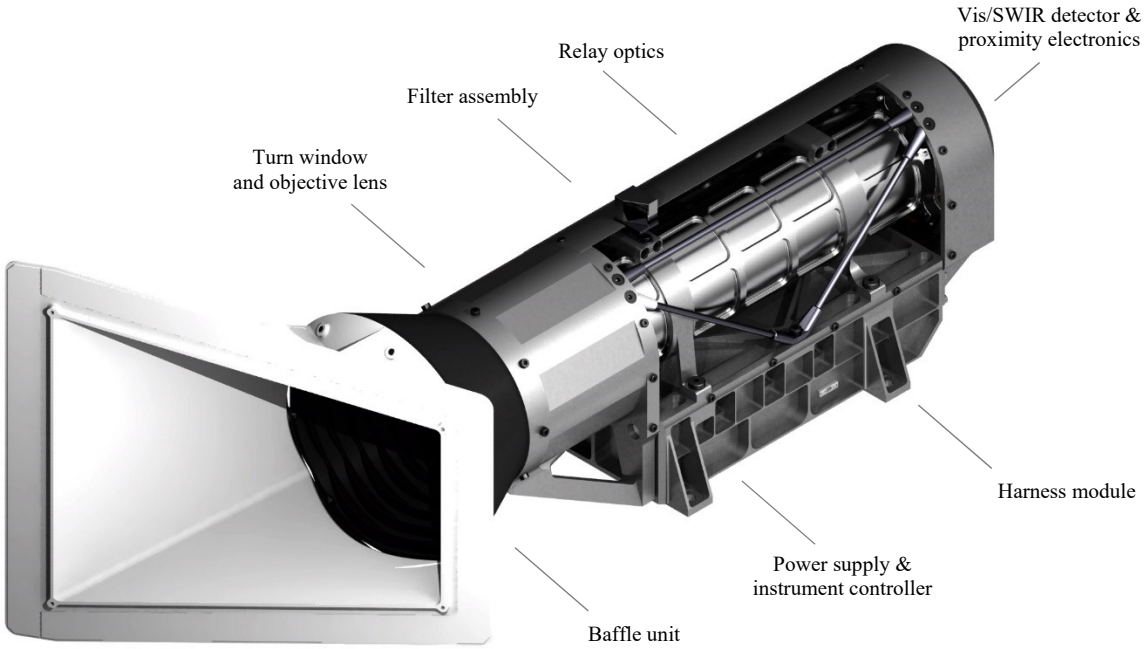

Figure 1. Render of the VEM configuration. Both instruments, VEM for VERITAS and VenSpec-M for EnVision, use the same optical setup and are structurally almost identical. Markers indicate the positions of the most relevant technical parts.

Radiation effect testing has become more challenging with decreasing structure size and increasing complexity on integrated circuits. In particular, the heavy-ion test for single event effects (SEE) faces various challenges. One is the availability of heavy-ion radiation with sufficient particle energy to reach the sensitive volume within such devices. Another is the complex integration and testing process to collect thorough data for a consistent interpretation.

In general, SEE testing focuses on device susceptibility due to single events e.g. single event latch-ups (SEL), transient overcurrent events (SET) or upsets (SEU) which could result in device destruction, but it also introduces permanent degradation due to the total ionizing dose (TID) and the displacement damage dose (DDD) within the crystal structure which mainly leads to an increased dark current and affects other key parameters like charge transfer, full well capacity or quantum efficiency.

Our goal is to space qualify the Xenics XWS-640 detector proposed for the VEM and VenSpec-M instruments. Therefore, irradiation data for the ion Linear Energy Transfer (LET) has to cover a range between 0 to 75 MeVcm²/mg which is needed to gain knowledge on the single event susceptibility and cross-section of a device to fulfill NASA/JPL led space qualification standards (≤ 75 MeVcm²/mg) as well as ESA space qualification standards (≤ 60 MeVcm²/mg) for heavy-ion irradiation.

2. HEAVY-ION TEST SETUP

2.1 Heavy-Ion Source RADEF

The RADEF Facility in the University of Jyväskylä in Finland is part of the European Network for radiation effect studies. They are ESA contractor since 2005 and therefore one of the main test facilities for European space industry in regard to SEE testing. The facility is specialized on high energetic heavy-ion cocktail and proton beams used to study radiation effects on semiconductor devices or new types of materials.

Radiation effects are separated into three distinct effect types, total ionizing dose (TID), displacement damage dose (DDD) and single event effects (SEE). The first two are covered either by proton irradiation or instead by gamma-ray and neutron irradiation. SEE is primarily covered by heavy-ion irradiation, although it also introduces TID and DDD.

For a thorough device study the ion penetration depth and the linear energy transfer (LET) are most sufficient. Therefore, RADEF offers four different cocktails of different specific energies to choose from.

The highest irradiation LET target for the sensor was 75 MeVcm^2/mg, thus a cocktail with specific beam energy of 16.3 MeV/n was used throughout the test campaign which offers various ion species from lower energetic Oxygen (^{17}O) up to high energetic Xenon (^{126}Xe) with respective penetration depths up to 500 µm for Oxygen and 150 µm for Xenon, which is sufficient for our device. The ions and tilt angles with their related parameters used throughout our test campaign are shown in Table 1. Note that introducing tilt reduces the ions lateral range normal to the device surface while increasing the LET.

Energy transfer of a specific ion is a function of its residual energy and therefore of the distance it has traveled through the lattice structure within a material. LET profiles for different ions and tilt angles used during irradiation have been modelled as a function of depth normal to the detector surface using the SRIM2013 tool [4]. These profiles are shown in Figure 2 below. The modelled detector layers are 200 nm of AR-coating, 5 µm InGaAs and 508 µm silicon ROIC. The AR-coating is of unknown material composition, so Al_2O_3 was assumed as it would match the spectral sensitivity of the detector. Since only the electro-optically active layers are susceptible to possible single events the energy loss within the first 20 µm of the detector are most relevant.

Table 1. Selected ions at beam energy 16.3 MeV/n used during irradiating the device under test (DUT) with the summarized SEL events. The LET @ SV denotes the sensitive volume of the ROIC.

Ion	Tilt [deg]	Energy [GeV]	LET @ DUT surface [MeVcm^2/mg]	LET @ SV surface [MeVcm^2/mg]	Range [µm (Si)]
$^{40}Ar^{14+}$	0	0.657	7.2	7.3	261
$^{57}Fe^{20+}$	0	0.941	48.5	49.8	209
$^{83}Kr^{29+}$	0	1.358	24.5	25.1	182
$^{83}Kr^{29+}$	45	1.358	34.0	36.0	127
$^{83}Kr^{29+}$	55	1.358	43.0	45.2	102
$^{126}Xe^{44+}$	0	2.059	48.5	49.8	153
$^{126}Xe^{44+}$	30	2.059	56.0	57.8	131
$^{126}Xe^{44+}$	47	2.059	74.0	75.0	107

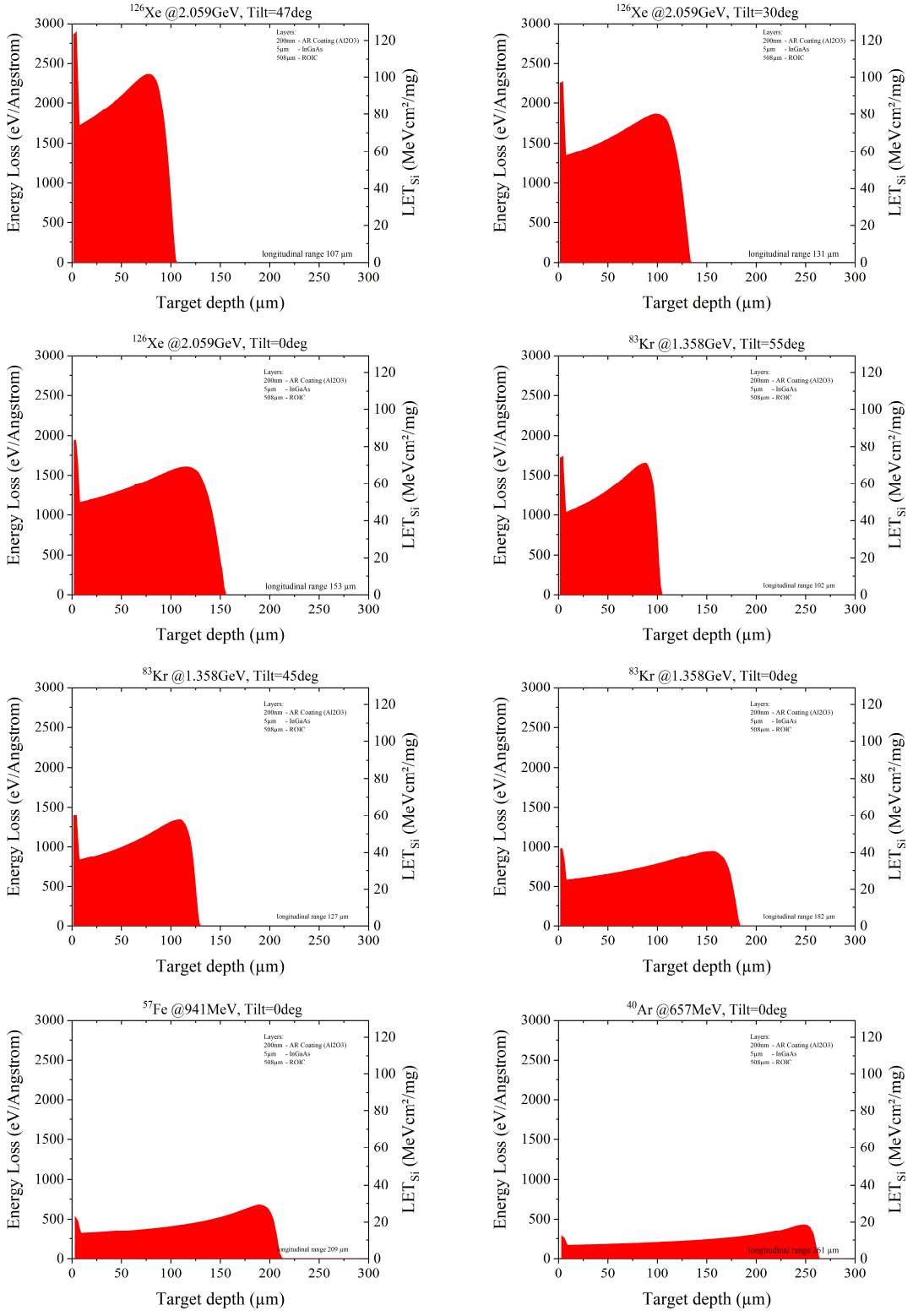

Figure 2. Longitudinal energy loss profiles of ^{126}Xe, ^{83}Kr, ^{57}Fe and ^{40}Ar and their respective incidence angle used during irradiation of the Xenics detector. After penetrating of the InGaAs layer with Xe at 47° tilt (top left) we reach a maximum LET of 75 MeVcm^2/mg or higher within the active detector volume.

2.2 Experimental Setup

To protect the detector during possible high current events we designed a PCB-extender as an interface between the detector and the original camera electronics. The PCB-extender's main functionalities are voltage switching, current monitoring and overcurrent protection. The design was built considering basic layout specifications as a proper stack-up, impedance control and length matching to have minimum signal degradation at the ADC inputs. External signals are supplied via a D-SUB-15 connector. The PCB-extender triggers an automatic turn-off of both detector voltages (VDDA and VDDD) in case of an overcurrent-event. Core elements of the latch-up protection are two flip-flops, that are set by the electrical ground support equipment (EGSE) and reset by the overcurrent-signals. An EGSE-PC controls and monitors the voltage enabling and status by an USB data acquisition system (DAQ). Figure 3 shows the assembled camera setup for the test with the detector on the left, camera electronics on the right and the PCB-extender connecting both parts.

There are two interfaces to control the test setup, one being the Camera-Link to the camera and the DAQ module. The camera link enables the control of the detector and the acquisition of image data. By the other hand, the DAQ monitors the detector input voltages and currents, and controls the power delivery and sequence by software. The power-supply for the camera-electronics is controlled via RS-232 interface.

Image acquisition and detector configuration was done with an EGSE-software developed in C++. The control of the camera-power and the monitoring of the detector-currents have been done by a dedicated software developed with National Instruments LabWindows. During transport and handling the detector was covered by a protective acrylic glass lid that was removed during irradiation.

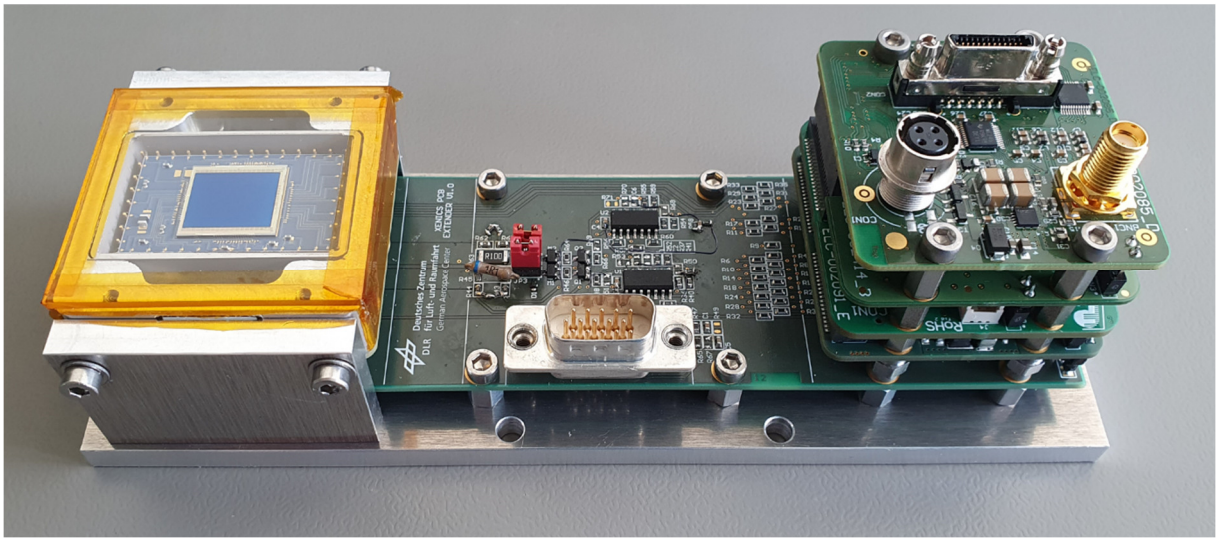

Figure 3. Assembled Camera setup with extension board for latch-up protection and high current monitoring, the sensor is on the left covered by an acrylic glass lid, the camera electronics on the right.

3. RESULTS

The irradiation measurements have been performed at +10°C sensor temperature, which is the nominal and single operational temperature at which the detector will be controlled in flight. Measurement data and their respective cross-section fit curve is shown in Figure 4. The error bars represent a 95% confidence level and 10% fluence accuracy. The data fitting does not perfectly match the measurement data, in particular for very low LET values. This possibly suggests the combination of two or more SEL-types, one of them characterized by lower LET threshold and lower saturated cross-section. This possibility shall be investigated during the full characterization of the Xenics detector, trying to measure amplitude, duration and shape of latch-up events on all the relevant lines. If the envelope (dashed line in Fig. 4) of two cross-section curves is used for data-fitting to one single curve, this leads to a conservative estimation of the SEL rate, because the envelope is always larger than the sum.

Table 2. Total ion fluence and the related number of SELs during irradiation.

Ion	Tilt [deg]	Fluence [cm-2]	# SEL [-]
$^{40}Ar^{14+}$	0	1.00E+07	1
$^{57}Fe^{20+}$	0	1.00E+07	3
$^{83}Kr^{29+}$	0	1.82E+05	8
$^{83}Kr^{29+}$	45	4.05E+04	7
$^{83}Kr^{29+}$	55	2.57E+04	10
$^{126}Xe^{44+}$	0	1.97E+04	9
$^{126}Xe^{44+}$	30	2.20E+04	9
$^{126}Xe^{44+}$	47	1.33E+04	7

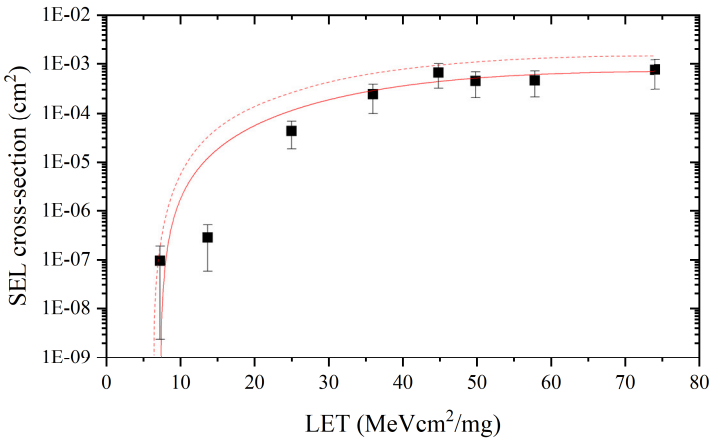

Figure 4. Estimated SEL cross-section curve for the Xenics XSW-640 detector.

Considering a curve which is the envelope of all the measured data as part of a single type of SELs represents a conservative approach (max subtended area). The rounded Weibull parameters of this envelope curve are shown in Table 3 below.

Table 3. Expected number of SEL for Xenics XSW-640 at +10°C, FoS included.

Parameter	Value
LET threshold [MeV·cm2·mg-1]	7
Saturated cross-section [cm2]	1.3e-03
Shape factor S [-]	1.9
Curve width W [MeV·cm2·mg-1]	70

Utilizing the parameters from Table 3 it is possible to provide a rough estimation of the expected number of events in flight during operations.

The number of latch-ups predicted by SPENVIS, expected during the whole 8.6-year mission (transfer trajectory + mission duration at Venus), factor of safety (FoS) and calculated duty cycle included, are given in Table 4 below [5, 6]. The worst-case event rates calculated for the worst 5-minutes-average peak are given in Table 5.

Table 4. Expected number of SEL for Xenics XSW-640 at +10°C during 5 years mission duration, FoS included.

Effects	Factor of Safety	Expected number of SEL
By direct ionization	2	0.70
By protons	10	0.18
Total	12	0.88

Table 5. Expected SEL rates (worst 5-minutes peak) for Xenics XSW-640 at +10°C, FoS included.

Effects	Factor of Safety	Expected rate of SEL [#·s-1]
By direct ionization	2	7.82e-06
By protons	10	3.52e-06
Total	12	1.13e-05

Blinking pixels struck by a particle shower as well as infrequent saturated lines or saturated images have been observed during heavy-ion irradiation. Because the FPA design includes a latch-up protection an SEL therefore is non-destructive, though a short power cycle may be necessary after each event.

The present estimation is affected by a relative low accuracy in the cross-section curve. More extensive tests with a full characterization of the Xenics XSW-640 sensitivity, with more test items and larger fluences, is planned to be performed in the close future. With the currently expected very low number of SEL, the Xenics XSW-640 can already be declared suitable for the mission - at least in terms of SEL hardness.

3.1 Dark Current

As a measure of the sensor degradation induced by the TID and DDD during irradiation, we compared the dark currents before and after the irradiation campaign in the high gain mode which will be used during the mission. Single pixel dark currents were summarized in a histogram and then fitted by a skewed Gaussian, which combines the Gaussian distribution and the error function as $F(x) = 2AG(x')E(\alpha x')$, with A the amplitude, $x' = (x - x_0)/\sigma$ and α the positive or negative skew. The respective peak position was then used as the representative sensor dark current.

The evolution of the dark current distribution on the sensor at 10°C temperature is shown below in figure 5 with their respective fits. During heavy-ion irradiation the pixel dark current distribution is transformed and skewed to the right ($\alpha > 0$) due to an increasing number of pixels with higher than average values. This degradation behavior was expected based on publications discussing the effects of radiation-induced displacement damage in InGaAs detectors [7]. The average dark current increased from around 100 ke/s to around 2 Me/s which constitutes to an increase factor of 20 (see Figure 8).

It is well known that there is an increased sensitivity of InGaAs photodiodes to displacement damage compared to silicon-based technology which is relevant for the increased dark current here [8].

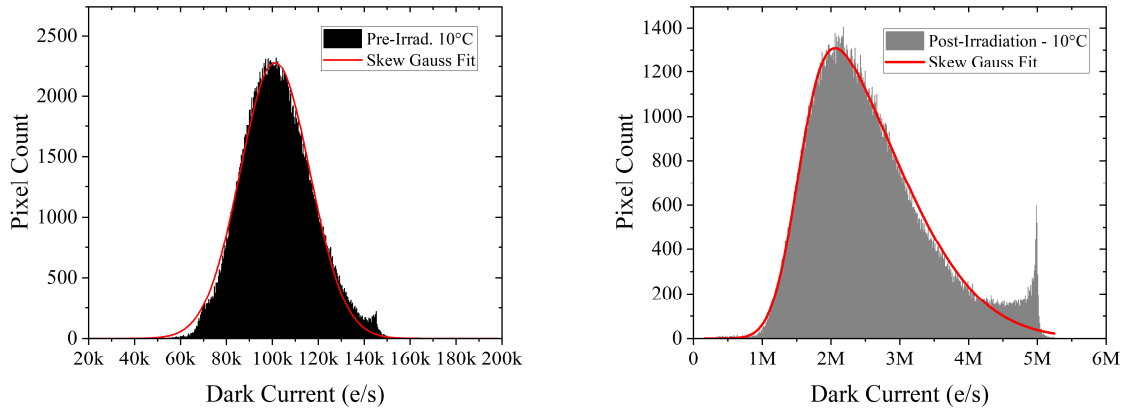

Figure 5. Evolution of the dark current distribution of the pixels before and after heavy-ion irradiation at 10°C sensor temperature. During irradiation the Gaussian distribution is transformed into a skewed Gaussian distribution.

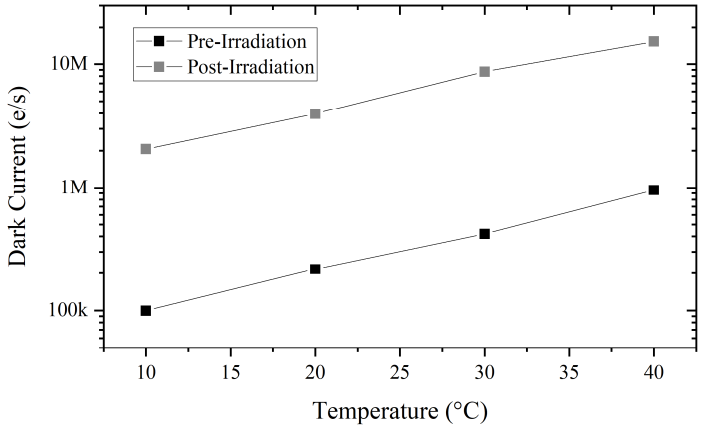

Figure 6. Dark current before and after the heavy-ion irradiation at different sensor temperatures in high gain mode.

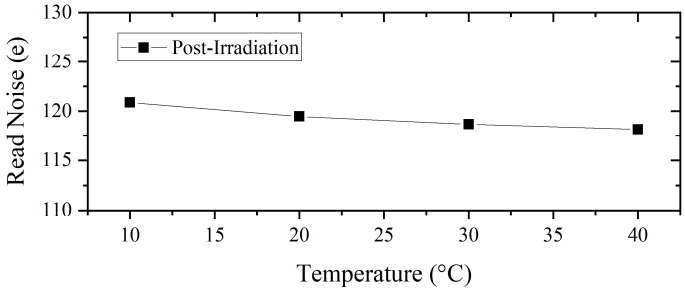

Figure 7. Read noise post-irradiation for the high gain mode shows no deviation from data sheet specifications (120 e/s).

Post irradiation dark currents were tracked over the course of 6 months with regard to room temperature annealing which was not observed. This is consistent with observations on InGaAs detectors made by others, with even higher temperatures [9, 10]. No reduction of the dark current was observed even after several hundred hours annealing at 85°C [7].

Read noise is not affected by the irradiation and shows no signs of increase compared to the specifications of 120 e/s typical in the high gain regime. Figure 7 shows the measured read noise at four different temperatures with average values between 118 and 121 e/s.

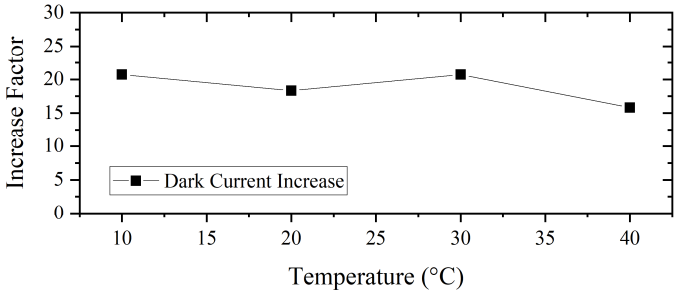

Figure 8. Dark current increase factor post-/pre-irradiation.

From these data we can calculate the damage factor that is commonly used to compare degradation of the device by dividing the dark current increase with the applied fluence [11].

$$K(\phi) = \frac{\Delta I}{\phi} = \frac{I_{irrad.} - I_0}{\phi} \quad (1)$$

For the estimation the Total Fluence [N]=2.04E+07 and the TID [rad]=3.47E+03 that were accumulated on the sensor over the full test procedure were used. We acquired an average fluence dependent damage factor of K~ 4.6E-2 e/s/N, which represents the dark current increase per incoming particle. By taking the TID we get a damage factor of ~2.7E+2 e/s/rad. The damage factor K depends on particle type and energy which are not resolved in our test.

3.2 Single Event Upsets

Heavy-ions and potentially high LET protons are known to introduce transients and upsets. In particular during irradiation at RADEF we captured live images with a frequency of 10 Hz and were able to directly observe the influence of the ion bombardment.

The most common SEU type is represented by the sudden increase of the luminosity in a single pixel, which lasts for a single image and quickly returns to nominal luminosity level. More rarely, a cluster of pixels (up to 5x5) can experience the same behavior, presumably due to a heavy ion impact creating a shower of electrons within the affected area. An example, taken with a surface LET = 74 MeV·cm^2·mg^{-1} (Xe tilted at 47°; flux of 100 ions/s) which featured a relative high number of blinking pixels with an impact cluster as well as partial single pixel excitations in the surrounding area, is shown in Figure 9.

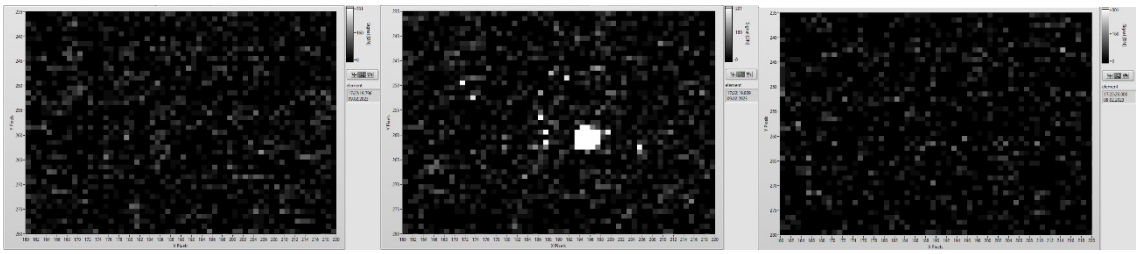

Figure 9. Zoomed view in a sequence of three consecutive images with an event and some “spill-over” during irradiation with Xe (surface LET=74 MeVcm^2/mg). The pixel cluster and all other affected pixels immediately return to their initial state without visible damage.

4. NEXT STEPS

The next step will be a proton test on a new set of identical detectors. This test will be carried out at the HZB Berlin-Wannsee. Depending on the outcome of this test and the present degradation level of the detectors we will try to perform high temperature annealing with respect to a potential implementation in flight.

5. CONCLUSION

For NASA's VERITAS mission and ESA's EnVision mission targeting Venus during the next decade we contribute a SWIR camera system with an InGaAs imaging sensor that is currently amid its space qualification campaign. We have tested the detector behavior under heavy-ion bombardment at the RADiation Effects Facility (RADEF) at the university of Jyväskylä, Finland. The radiation test has been successfully performed and our test goals have been achieved. Our data covers a LET range up to 75 MeVcm²/mg needed to fulfill NASA/JPL and ESA led space qualification standards for heavy-ion testing. Data about SEL sensitivity has been gathered and the images acquired during irradiation provided an indication of the SEU types expected during the missions. An average TID dose damage factor of ~2.7E+2 e/s/rad is expected. During irradiation, the sensor has correctly been maintained at the planned mission temperature of +10°C. Comparing pre- to post-irradiation dark currents our data shows an increase factor of around 20. No room temperature annealing was observed. Finally, the detector showed saturated cross-sections below 1E-3 cm² at 10°C with acceptable event rates for the highest LETs.

6. ACKNWOLEDGEMENTS

VERITAS and EnVision are NASA/JPL and ESA missions respectively. The VEM instrument for VERITAS and the VenSpec-M instrument for EnVision are being developed by DLR with French contribution of the optics from CNES and LESIA.

REFERENCES

[1] Helbert, J., et al., The Venus Emissivity Mapper: implementation for flight on the NASA VERITAS mission, Infrared Remote Sensing and Instrumentation XXX. 10.1117/12.2634263 (2022).
[2] Helbert, J., et al., The VenSpec suite on the ESA EnVision mission to Venus. EGU General Assembly, Vienna, Austria (2019).
[3] Xenics XSW-640, Datasheet (2023).
[4] Ziegler, J. F., Biersack, J.P., "The Stopping and Range of Ions in Matter.", In: Bromley, D.A. (eds) Treatise on Heavy-Ion Science, Springer, Boston, MA. https://doi.org/10.1007/978-1-4615-8103-1_3 (1985).
[5] Messenger, S., et. al, NIEL for Heavy Ions: An Analytical Approach, IEEE Transactions on Nuclear Science, 1919-1923 (2003).
[6] Truscott, P., "JORE2M2 Project: SHIELDOSE-2Q Software User Manual," QINETIQ/TS/AS/SUM1003576 (2010).
[7] Tauziede, L., et al., Evaluation of InGaAs array detector suitability to space environment, Proceedings Volume 10564, International Conference on Space Optics — ICSO 2012; 105640O (2017).
[8] Gilard, O., et al., Damage Factor for Radiation-Induced Dark Current in InGaAs Photodiodes, IEEE Transactions on Nuclear Science, 65 (3), 884-895 (2018).
[9] Barde, S. et al., Displacement Damage Effects in InGaAs Detectors: Experimental Results and Semi-Empirical Model Prediction, IEEE Transactions on Nuclear Science, 47(6), 2466-2472 (2000).
[10] Amore, O., et al., InGaAs SWIR imaging detectors hardening against proton irradiation, Infrared Technology and Applications XXVIII, 436 (2003).
[11] Srour, J., et al., Universal damage factor for radiation-induced dark current in silicon devices, IEEE Transactions on Nuclear Science, 47 (6), 2451-2459 (2000).